Constitutive Model for Numerical Modelling of Highly Stressed Heterogeneous Massive Rocks at Excavation Boundaries

M.C. Villeneuve
Jacobs Associates, San Francisco, USA

M.S. Diederichs
Queen's University, Kingston, Canada

P.K. Kaiser
Laurentian University, Sudbury, Canada

C. Frenzel
Herrenknecht AG, Schwanau, Germany

ABSTRACT: A numerical modelling approach was developed to explicitly simulate geomechanical characteristics of intact rock: mineralogy, grain size and fabric. The approach involved creating a representative constitutive model for each of three common rock-forming minerals: mica, quartz and feldspar. The constitutive models developed are valid within the low confinement realm of excavation boundaries, where tensile fracture processes dominate. The mineral types were assigned to numerical elements, which were associated with each other through an algorithm created in a finite difference model, FLAC 2D (Itasca 2007a), to simulate real crystal geometries and orientations. The numerical models were used in a parametric investigation of the geomechanical characteristics and compared with published observations of the rock yielding process in laboratory testing. This approach has allowed the explicit grain-scale investigation of the impact of geomechanical characteristics on rock yielding at low confinement, leading to an improved mechanistic understanding of excavation-scale rock yielding processes at excavation boundaries.

1 INTRODUCTION

The numerical modelling approach consists of using simple numerical models and conducting a parametric analysis of various input parameters. The parameters under consideration are mineralogy, grain size and grain size distribution and foliation, requiring mineral-specific constitutive models. FLAC (Itasca 2007a) was designed primarily to accommodate whole-rock approximations, with some built-in variability in the input parameters for introduction of heterogeneity. This methodology has been successfully applied in numerical modelling (not only in FLAC) for investigations of rock failure in simple (Diederichs 2003, DeBorst 2002, Fang & Harrison 2002, Tang & Kaiser 1998, Zhu & Tang 2004) and complex tests (Liu et al. 2002a, Liu et al. 2002b).

Two-dimensional UCS and Brazilian tests were created in FLAC to investigate tensile fracture processes by focussing on initiators and receivers of tensile fractures (Fig. 1). Whether a mineral acts as an initiator or receiver of tensile fractures will depend on its strength, stiffness and dilation parameters, its geometry and alignment with the induced stress field, and the physical and geometrical properties of the minerals adjacent to it. To undertake this type of investigation, mineral-specific input parameters instead of whole-rock analogues are required, similar to other published work (Li et al. 2003), requiring considerable constitutive model refinement to assign appropriate constitutive models and input parameters for minerals. Published mineral-specific strength data, as well as parametric analysis and comparison to laboratory observations of fracture behaviour, were used to determine valid mineral-specific constitutive models. This model was created for crystalline rocks only, due to the difference in characteristics of grain boundaries found in sedimentary rocks. Ultramafic, volcanic and highly altered ore rocks are also not considered due to limited data in these rock types.
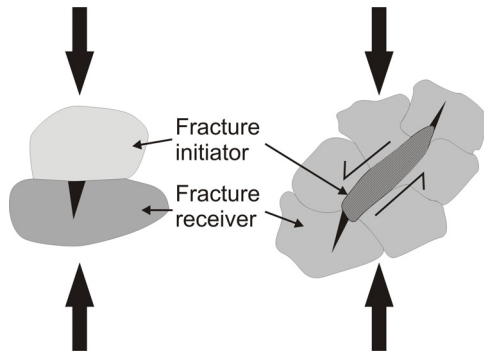
Figure 1: Schematic of fracture initiation and receiver relationship between minerals. Left: indentation; right: shear strain initiation in mica acting as shear zone.

2 INPUT VALUES FOR STRAIN SOFTENING CONSTITUTIVE MODEL

2.1 *Introduction*

Peak physical, elastic and laboratory strength properties for quartz, feldspar and mica are shown in Table 1. These published values were used as input values for peak portions of the FLAC strain-softening constitutive model in the UCS and Brazilian models. Although the strain-softening constitutive model allows change in parameter values with plastic strain, the stiffness moduli are independent of plastic strain. The majority of the published values, such as elastic, shear and bulk modulus, density and Poisson's ratio, can be used as-is in the constitutive model, but the cohesion, friction and tensile strengths are more difficult to directly relate between laboratory test values and modelling values. Difficulties arise from the differences in scale at which laboratory testing is undertaken compared with the scale of individual mineral grains in rock, which are reproduced in the numerical model. The terms parallel and perpendicular are used according to the direction in which the maximum principal stress will act on an individual mineral grain, as shown in Figure 2. Note that strength is weakest parallel to the basal planes, while stiffness is lowest perpendicular to the basal planes.
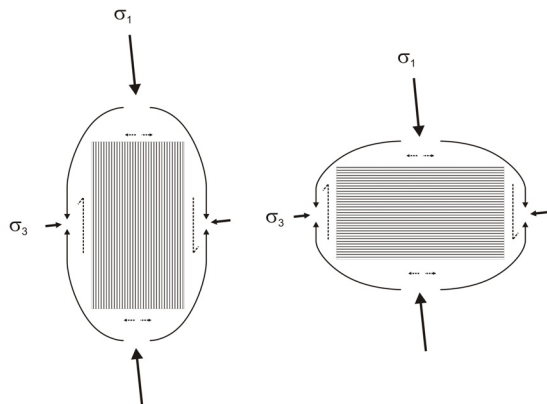
Figure 2: Schematic demonstrating vocabulary used in describing anisotropic mica strength and stiffness parameters. Parallel describes the stress state at left, while perpendicular refers to the stress state at right. All strength and stiffness parameters are related to which one will be invoked in the parallel or perpendicular stress state.

2.2 *Stiffness Moduli*

The stiffness moduli for minerals are listed in Table 1. The stiffness moduli for biotite were calculated using elastic constants for the crystal lattices, and demonstrate a large anisotropy due to the anisotropy along and against the basal planes.

Table 1: Average physical and elastic properties of three common rock-forming minerals.

Mineral	Density g/cm3	Young's Mod GPa	Shear Mod GPa	Bulk Mod GPa	Poiss. Ratio	UCS Strength MPa	Tensile MPa	Internal Friction Coeff.	Source
Quartz	2.72	-	-	-	0.2	329	34	-	*Blair, 1955
	2.8	58	23	-	0.29	-	-	-	*Ramana, 1973
	2.59	54	-	-	0.17	-	-	-	*Belikov, 1967
	2.47	38	-	-	0.21	-	-	-	*Belikov, 1967
	2.65	96	-	-	-	-	-	-	*Belikov, 1967
	-	47	-	-	-	167	-	-	*Cochrane, 1964
	-	44	-	-	-	172	-	-	*Cochrane, 1964
	-	68	-	-	-	-	-	-	Carmichael, 1982
	-	-	-	36	-	-	-	-	Birch, 1966
	-	73	31	38	0.18	-	-	0.25	Fukuhara et al.,1997
	-	-	-	-	-	254	-	-	Lama & Vutukuri,1978
Average	2.65	64	27	37	0.19	230	34	0.25	
Feldspar	2.61	75	30	-	0.27	-	-	-	*Belikov, 1967
	2.57	71	-	-	-	-	-	-	*Belikov, 1967
	2.7	89	35	-	0.28	-	-	-	*Belikov, 1967
	2.7	89	-	-	-	-	-	-	*Belikov, 1967
	2.55	75	29	-	0.27	-	-	-	*Belikov, 1967
	2.61	77	30	-	0.29	-	-	-	*Belikov, 1967
	2.61	77	-	-	-	-	-	-	*Belikov, 1967
	2.54	63	24	-	0.29	-	-	-	*Belikov, 1967
	-	96	-	-	-	-	-	-	Angel et al., 1988
	-	-	-	47	-	-	-	-	Birch, 1966
	-	-	-	52	-	-	-	-	Birch, 1966
	-	-	-	49	-	-	-	-	Birch, 1966
	-	-	-	57	-	-	-	-	Birch, 1966
	-	91	-	-	0.33	230	-	-	*Belikov, 1967
	-	-	-	-	-	290	-	-	Lama & Vutukuri,1978
Average[1]	2.61	80	30	51	0.29	260			
Mica	2.75	20	-	-	-	150	-	-	*Corns & Nesbitt 1967
	3.1	70	28	-	0.28	-	-	-	*Belikov, 1967
	-	53	6	-	-	-	-	-	Birch, 1966
	-	179	77	-	-	-	-	-	Birch, 1966
	2.79	80	32	-	0.25	-	-	-	*Belikov, 1967
	-	-	-	52.	0.26	-	-	-	Birch, 1966
	-	53	12	-	-	-	-	-	Birch, 1966
	-	147	68	-	-	-	-	-	Birch, 1966
	2.78	61	-	-	-	112	-	-	*Coates,Parsons1966
	-	177	70	-	-	-	-	-	Mcneil,Grimsditch,1993
	-	61	15	-	-	-	-	-	Mcneil,Grimsditch,1993
Average -parallel	2.86	98	38	52	0.26	131.0			
		168	72						
-perpend.		56	11						

[1] Not enough data for directionality wrt cleavage planes   * Summarised in Lama & Vutukuri (1978)

Due to the extreme anisotropy, the stiffness moduli relationships between Young's, Bulk and Shear modulus and Poisson's ratio do not hold true for micas, and the shear modulus and bulk modulus must be calculated using the elastic constants in each crystal direction. The anisotropy in stiffness is only addressed by the Young's modulus, which is not a parameter in FLAC, while both shear and bulk modulus are the same in either direction in 2-D.

2.3 Friction Determination

In modelling mineral failure the confinement dependent portion of strength provides strength to an element under stress, and is akin to the lattice friction, an intrinsic property of the mineral.

With large deformation and damage to the mineral surfaces, the microfracture surfaces are more akin to a gouge, and the friction coefficient is likely similar to the values determined by Morrow et al. (2000). For this reason, two coefficients are used to reflect this change in phase: the mineral surface coefficient of friction measured by Horn & Deere (1962) to simulate the lattice friction, and the friction coefficient of gouge to simulate damaged mineral friction (Fig. 3).

Roughened mineral surfaces were found to have higher coefficients of friction than their polished counterparts (Horn & Deere 1962), suggesting that mineral-specific coefficients of friction may have an additional term to account for the interlocking of asperities due to microfracture scale roughness. In the case of rock, this term is normally called i and is the angle of inclined surfaces over which the fractures must slide during displacement, measured as the ratio of the amplitude to the wavelength of the fracture surface (Patton 1966).

Intragranular microfractures are assumed to have the same friction coefficient to roughness coefficient, i, relationship as macrofractures in polycrystalline rock. Equation 1 is used to combine both aspects of friction and is assumed to be valid at low strains, where failure through the asperities is not of concern. This assumption is not to be confused with relationships governing microfractures or macrofractures through polycrystalline rock.

$$\tau = \sigma_n \tan(\phi_b + i) \tag{1}$$

where σ_n is the normal stress, ϕ_b is the basic friction angle and i is the angle of the saw-tooth fracture surface (Patton 1966). The mineral base friction is made up of the lattice friction and the microfracture surface roughness coefficients (Fig. 3):

$$\phi_b = \phi_l + i_l \tag{2}$$

An analysis of the ratio between amplitude and length of the microfractures present in the quartz grains (Fig. 4a-c) of Stanstead granodiorite was conducted and shows that the i_l ranges from 1-1.5^o, giving a tan(i_f) 0.018 to 0.028. This is only slightly more than a 10% increase in the base friction coefficient value given in Table 2. Figure 4d-f shows the nature of intragranular microfractures in mica and feldspar, in Leventina gneiss, which tend to be parallel to, or perpendicular to cleavage, which in all images in Figure 4d-f is parallel to the long axis of the mineral grain. The cleavage parallel microfractures are very smooth, giving an i_l of 0, while the cleavage perpendicular microfractures follow a more tortuous path (Fig. 4e-f), giving an i_l of approximately 25° and a tan(i_f) of 0.47. Where cleavage parallel and perpendicular microfractures in mica coalesce, they form a microfracture with large amplitude (Fig. 4a), giving an i_l of approximately 15°, and a tan(i_f) of 0.27. According to these measurements, the mineral base coefficient of friction is lower than the gouge coefficient of friction for quartz and cleavage parallel microfractures in mica and feldspar, or higher than the gouge coefficient of friction for cleavage perpendicular microfractures in mica and feldspar.

The obstruction to shear strain during mineral failure arising from tortuous intragranular microfractures suggests that the resultant 'friction angle' is much higher than i_l. This value would be very difficult to measure, but evidence supporting this hypothesis was found by Diederichs (1999), where an input grain-specific friction angle of 45° was necessary to obtain a whole-rock friction angle approaching 30° during biaxial testing in 2-D particle flow code (PFC, Itasca 2007b) models. Based on these findings, a nearly instantaneous (at $\varepsilon = 1\times10^{-8}$) 'friction angle' gain of 45° is used in 2-D FLAC models. This simulates the instantaneous transition from a continuous array of mineral elements to the discontinuity caused by fracture generation, since FLAC does not create discrete fractures when an element (or grain) fails. The value of 45° was selected based on the need to obtain a considerable change in results between the delayed friction gain and instantaneous friction gain, although the true value is not currently known, and because of time considerations was not tested. The initial friction remains the same as that quoted in Table 2 to ensure that the element failure occurs at the appropriate stress level. The instantaneous increased friction angle simulates the initial interlocking friction at steep discontinuity asperity slopes. Although fractures generated along the cleavage mica plane have rare asperities and should not have instantaneous friction gain, in order to prevent numerical instability caused by intense strain localisation along ubiquitous joints, an instantaneous increased friction angle was also applied to the mica ubiquitous joints.
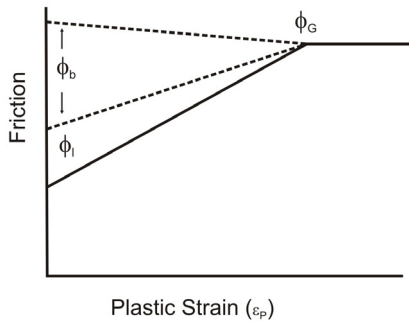
Figure 3: Schematic of plastic strain dependence of friction coefficients of mineral surface phase and mineral gouge phase, showing lattice, ϕ_l, and base, ϕ_b, coefficients of friction.
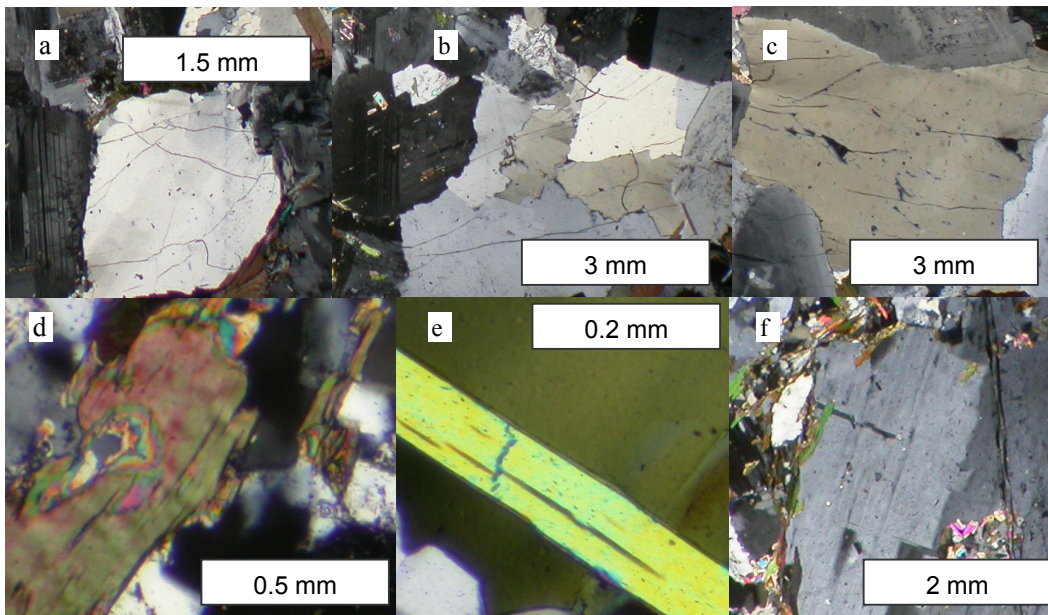
Figure 4: Photmicrographs of intragranular quartz microfractures (a-c), and intergranular microfractures in mica (d, e) and feldspar (f) used to determine microfracture roughness, i_l.

Table 2: Mineral-specific friction coefficients based on published and calculated values

Mineral	Individual Minerals				Mineral Gouges	
	Lattice ϕ_l	Roughness i_l	Base ϕ_b	Instantaneous ϕ_I	ϕ_G	
Quartz	0.12	0.012	0.132	1	0.65	
Feldspar	0.12	$0 - 0.47$	$0.12 - 0.59$	1	0.8	
Biotite	0.31	$0 - 0.47$	$0.31 - 0.78$	1	0.43	

Due to the anisotropy in the microfracture roughness coefficient, the cleavage (basal plane) parallel and perpendicular values for mica were associated with the corresponding strength and stiffness parameters according to Figure 2.

2.4 Cohesion Determination

Cohesion was determined using the relationship between UCS, cohesion and coefficient of friction, according to:

$$c = \frac{UCS(1 - \sin\phi)}{2\cos\phi} \tag{3}$$

Using the published values for UCS for minerals, as well as mono-mineralic rocks, in Table 1 and the base friction coefficient values for each mineral, calculated from the values in Table 2 using Equation 1, an estimate of peak cohesion was obtained. In a purely unconfined state the frictional component of strength would not be mobilized and cohesion would be estimated as half of the UCS strength, suggesting that using Equation 3 likely underestimates cohesion. Cohesion, however is a rock property as defined by the Mohr-Coulomb methodology, and independent of confinement. The use of Equation 3 is, therefore, the most appropriate approach to estimating the basic mineral strength parameters. The peak cohesion is a combination of base mineral friction coefficient and peak mineral UCS strength, while the residual cohesion is a combination of the static gouge and residual axial strength.

The cohesion for mica should be equally anisotropic as the tensile strength and stiffness moduli. The UCS values in Table 1 do not specify whether or not they are parallel or perpendicular to the basal plane, but judging by the Young's modulus values quoted along with the UCS values, they appear to have been tested parallel to the basal plane. Taking the same UCS to tensile strength ratio as for quartz and feldspar, all of which reflect failure through covalent bonds, the UCS perpendicular to the basal plane could be as high as 390 MPa. For the purposes of this research, this was used as the UCS strength estimate perpendicular to the basal plane, and perpendicular peak cohesion was calculated based on this value.

2.5 *Tensile Strength*

The tensile strengths for minerals are listed in Table 1. The stiffness of micas was shown in Section 2.2 to be highly anisotropic, in particular in the directions parallel and perpendicular to the mineral basal planes. The same should hold true for tensile strength. In the absence of mica data, this is based on graphite data, another platy mineral with perfect cleavage, and a 1:10 ratio of parallel to perpendicular fracture toughness (Tromans & Meech 2004). The strong covalent bonding between mica tetrahedra and octahedra (McNeil & Grimsditch 1993) is similar to that between carbon atoms in graphite. If graphite can be used as an analogy for mica, then a similar ratio should also exist for mica, resulting in a max. perpendicular tensile strength of 39MPa.

2.6 *Dilation Parameter Determination*

Although brittle rock failure is highly dilatant (Diederichs 2003), the determination of the dilation parameter for brittle rocks is difficult and anisotropic. Several rules of thumb exist for isotropic dilation, including the associated flow rule (where the dilation parameter is equal to the coefficient of friction) in both tensile and shear failure (Itasca 2007a). They are all based on continuum models and are not directly applicable to brittle rock failure. Dilation can range from 0 to the coefficient of friction according to continuum model methods and determining the exact value is still unclear. For the purposes of this research, a dilation angle of 15% of the initial friction angle is for tensile, uniaxial and biaxial failure.

2.7 *Grain Boundaries*

Grain boundaries are a special system within a mineral grain in that they can act as both crack initiators and crack arrestors. Their low stiffness (Diederichs 1999), due to lattice misalignment (Fig. 5) between similar mineral types or incompatible lattices between different mineral types, allows them to arrest intragranular cracks. When oriented oblique to maximum stress direction or parallel to maximum stress direction within the stress field, their lower cohesion and tensile strength; allows them to act as crack initiators. Grain boundaries have been found to contain large concentrations of microfractures in undeformed samples (Moore & Lockner 1995), contributing to lower strength (Nasseri et al. 2005, Nasseri et al. 2002). The lower density (Tromans & Meech 2002) leads to lower strength and stiffness. For this reason, the grain boundaries in the FLAC model are given separate, but related, input parameters to reflect these property differences. These properties depend on the two mineral types adjacent to the boundary, and follow these rules of thumb: stiffness is half the stiffness of the softer mineral, cohesion and tensile strength are 85% of the average strength between the two minerals, and friction is whichever friction coefficient is lower. The strength-strain relationships follow the relationship in Eq. 4.
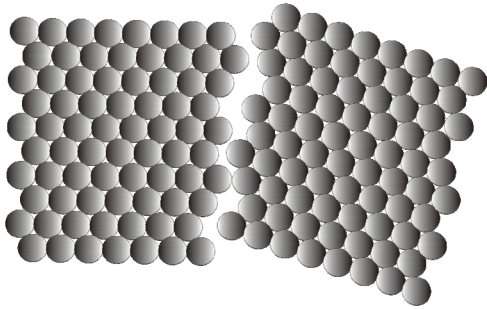
Figure 5: Schematic of lattice misalignment at grain boundaries.

3 VERIFICATION OF CONSTITUTIVE MODEL

3.1 *Laboratory Testing Dataset*

A dataset of UCS, triaxial and Brazilian strength tests on samples from Stanstead granodiorite (courtesy: J. Archibald) was used as a baseline with which to verify the mineral-specific constitutive models as well as the texture creation algorithm. This granodiorite is composed of 70% feldspar (potassium feldspar and plagioclase), 20% quartz, and 9% mica and 1% of other accessory minerals. The grain sizes range from medium to coarse, 2-16mm, individual grains are rounded, to slightly elongated, although they do not define an anisotropic fabric. The mineral type, grain size and grain orientation distribution are isotropic (Fig. 6).

3.2 *Numerical Modelling Calibration Results*

The texture and mineral composition of the Stanstead granodiorite were created in the FLAC model (Fig. 7) and used in both the UCS and Brazilian test models, using the texture algorithm described in Villeneuve et al. (2009). A series of numerical uniaxial and biaxial tests, as well as Brazilian tests were conducted and compared to the averaged laboratory test data.

3.2.1 *Brazilian Tensile Testing*

The Brazilian tensile strength of Stanstead granodiorite was found to be 6.5MPa (courtesy J. Archibald). This value is low with respect to the UCS strength and the rock type. Examination of thin sections showed that 70% of the quartz grains contain intragranular and transgranular microfractures extending only within adjacent quartz grains, as shown in Figure 4. This was also observed by Nasseri et al. (2002) in granitoids and led to decreased fracture toughness values since pre-existing microcracks can be used to link new induced microcracks and eventually lead to rupture (Moore & Lockner 1995). Results from numerical Brazilian tensile testing using high end tensile strength values from Table 1 give a Brazilian tensile strength of 16 MPa. By decreasing the input tensile strength for quartz to 2 MPa the Brazilian tensile strength of the modelled granodiorite is approximately 8.5-9.2 MPa, while 15% dilation increases this strength to approximately 9.3-11.3 MPa, which is slightly higher than the physical test strength and within three standard deviations of the dataset.

A comparison of the input tensile strength values required to obtain a fit to the Brazilian tensile strength of the Stanstead granodiorite reveals:

1. The input tensile strength is much higher than either the Brazilian tensile strength or the tensile failure stress at which the elements fail. This suggests that Brazilian tensile strength cannot be directly estimated based on the mineral-specific input tensile strengths, as the estimates would be unrepresentatively high.
2. Damage to even a small percentage of the minerals (70% of quartz, which comprise only 20% of the composite) can greatly lower the Brazilian tensile strength, demonstrating that pre-existing damage, either due to sampling or tectonic history, causing intragranular microfractures at the grain scale is important for Brazilian tensile strength and should be taken into account when characterising rock.

In addition to the input tensile strength, the heterogeneity in stiffness moduli arising from the different minerals and their grain boundaries is critical to obtaining a fit to the Brazilian tensile

strength of the Stanstead granodiorite, as seen in laboratory testing of Westerly granite (Tapponier & Brace 1976, Wong 1982). Tests run with homogeneous stiffness moduli resulted in Brazilian tensile strengths of 44 MPa and 60 MPa for low and average input tensile strengths, respectively. These values are clearly too high, and no amount of lowering the quartz tensile strength and cohesion could reduce the Brazilian tensile strength to fit with the Brazilian tensile strength of Stanstead granodiorite. In addition to the strength difference, the yielding behaviour is also different. If homogeneous stiffness moduli are used, the failure is distributed throughout the sample, while with heterogenous stiffness moduli, the failure is constrained within discrete yielding planes, interpreted as macrofractures (Fig. 8).
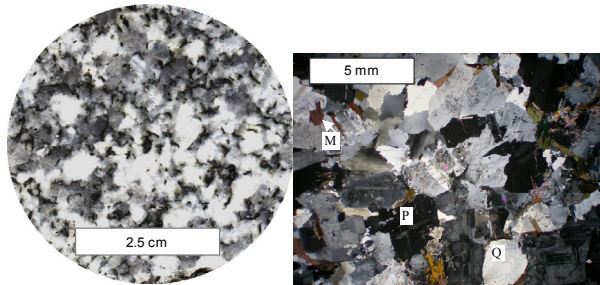
Figure 6: Photo and photomicrograph of Stanstead granodiorite showing isotropic nature of the material. Q=quartz, P=feldspar, predominantly plagioclase, M=mica, predominantly biotite.
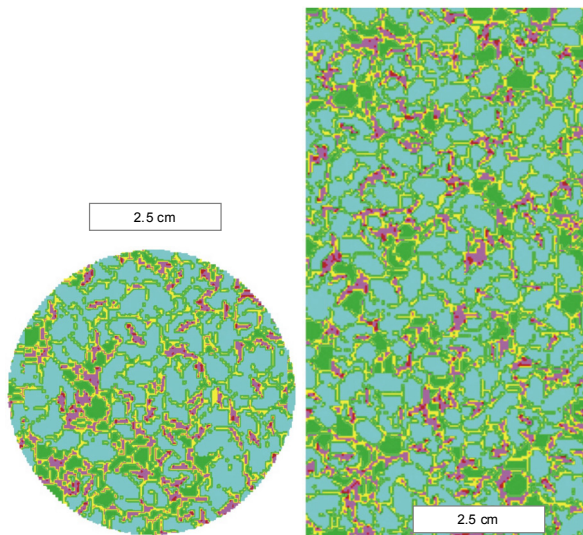
Figure 7: Images of modelled Stanstead granodiorite in FLAC. Colours relate to mineral type as follows: turquoise = feldspar, green = quartz, red = mica, yellow = grain boundaries.
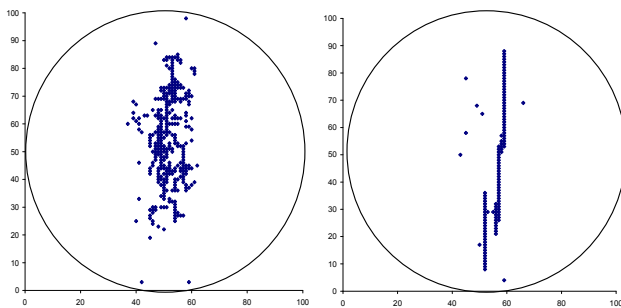
Figure 8: Locations of element failure leading up to composite sample failure for samples with homogeneous (left) and heterogeneous (right) stiffness moduli; all other input parameters are identical.

3.2.2 *UCS and Biaxial Testing*

The goal of the UCS and biaxial model testing was to duplicate the UCS and triaxial values obtained from laboratory testing of the Stanstead granodiorite (courtesy J. Archibald). Based on the laboratory triaxial data, linear curve fitting of the Mohr circles joining $\sigma_3 - \sigma_1$ data the cohesion and friction angle were estimated for two instantaneous confining stress values: 5 MPa and 10 MPa. The fit lines give friction angles, ϕ, of 64° and 62.5 ^{o}, and friction coefficients of 2.05 and 1.92, respectively. These are higher than the highest coefficient of friction of any of the individual minerals and mineral gouges. The shear stress intercepts gave cohesion values of 28 MPa and 41 MPa, respectively. These values are excessively high (for friction) and low (for cohesion) due to the limited range of data points restricted to low confinement $\sigma_3 < 0.1\sigma_1$.
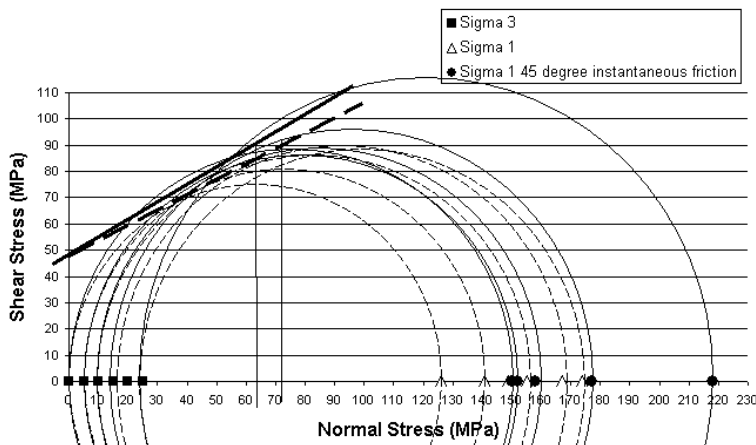
Figure 9: Mohr-Coulomb graph of biaxial test s1 and s3 data for modelled Stanstead granodiorite with delayed friction (dashed lines) and with instantaneous 45o friction (solid line) with Mohr circles and estimated Mohr-Coulomb parameter fits.
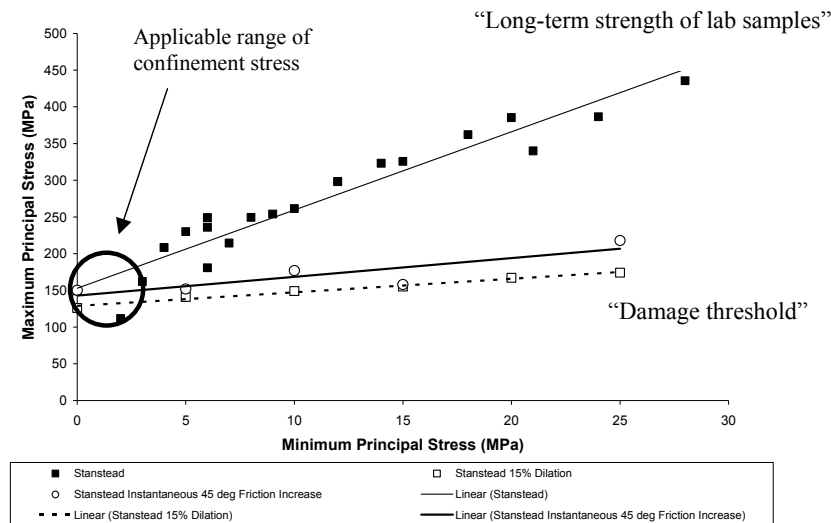
Figure 10: Peak strength envelopes for Stanstead lab test data (courtesy of J. Archibald), Stanstead model data with 15% dilation and Stanstead model data with 15% dilation and instantaneous friction increase.

The biaxial tests were modelled using average strength parameters, low tensile strength and instantaneous friction gain to 45°. The resulting biaxial strengths are plotted in Fig. 9 and show that the composite rock friction angle is 33.5^{o} and the coefficient of friction is 0.66, with a cohesion value of 47.5 MPa. The upper envelope (applicable at higher confinement) is analogous to the lab values with instantaneous, while the lower envelope (applicable at low confinement) is analogous to the model values with delayed friction gain. The constitutive model used for UCS and Brazilian tensile modelling follows Figure 10, and generates the most realistic results.

3.3 *Summary of Fracture Behaviour*

The mineral-specific behaviour described in the literature (Li et al. 2003, Li 2001, Tapponier & Brace 1976, Wong 1982) was also observed in the 2-D FLAC UCS and Brazilian models. The micas, being soft in shear (Fig. 11a, centre right), induce failure in the surrounding stiffer, stronger, feldspar (Fig. 11a, centre left), as discussed in Li (2001). A tensile fracture propagating (but ultimately abandoned) through feldspar (Fig. 11a, lower right, circled in white) can be halted at the softer and weaker grain boundary (Fig. 11a, lower left, red circle), as shown by Martin (1994) and Li (2001). A tensile fracture propagating through feldspar (Fig. 11b, right showing strain due to tensile fracturing) can be offset by a more compliant mica grain (Fig. 11b, left showing deviation of fracture), which does not propagate the fractures well at a large angle to the cleavage, as in Tapponier & Brace (1976) and Li (2001). A macrofracture will eventually develop in uniaxial loading, and the fracture path will include all mineral types (Fig. 11c).
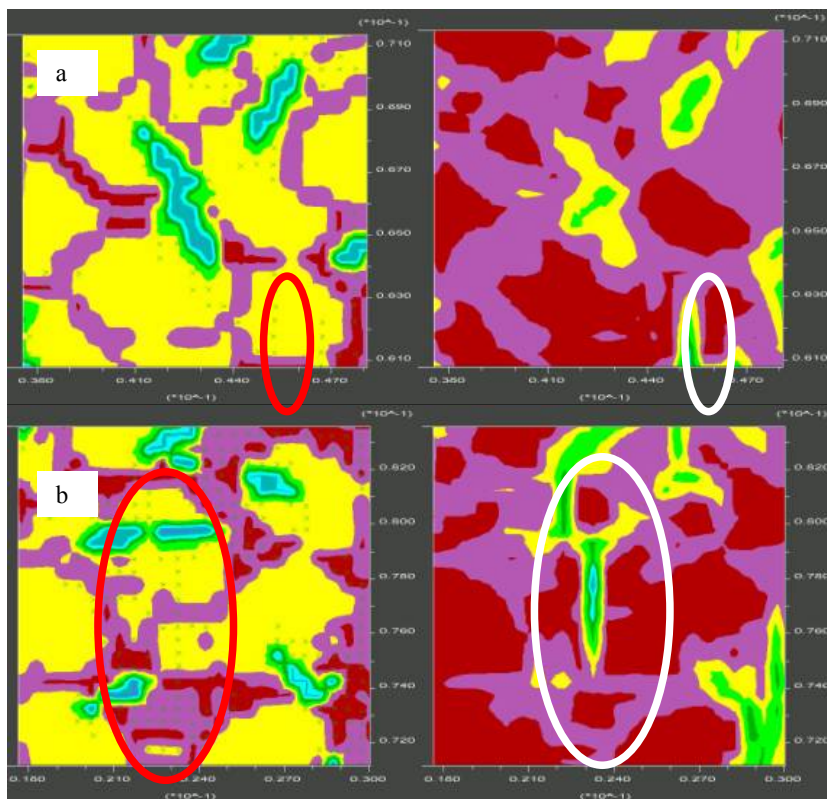
Figure 11: FLAC output of failed modelled Stanstead Granodiorite showing: a) induced failure around biotite (left) and the shear strain intensity of the corresponding region (right; yellow-green is higher strain); Red (left) and white (right) circles highlighting tensile fracture propagating through feldspar; b) induced tensile failure through feldspar, then moving around biotite (left) and the shear strain intensity of the corresponding region (right);

Tensile failure in a Brazilian test in FLAC is less dependent on fracture accumulation and coalescence than the UCS failure, since the tensile stress is generated at the centre of the sample and leads to tensile failure in the material of least resistance within the zone of tensile stress. Figure 11d shows the centre of a failed Brazilian model in which the failure began in a mica grain, and propagated up and down to form a nearly linear fracture surface. In this case, very little deviation by other minerals occurs, and the fracture propagates nearly unhindered. This is similar to the failure surfaces observed in laboratory Brazilian and point load tests.
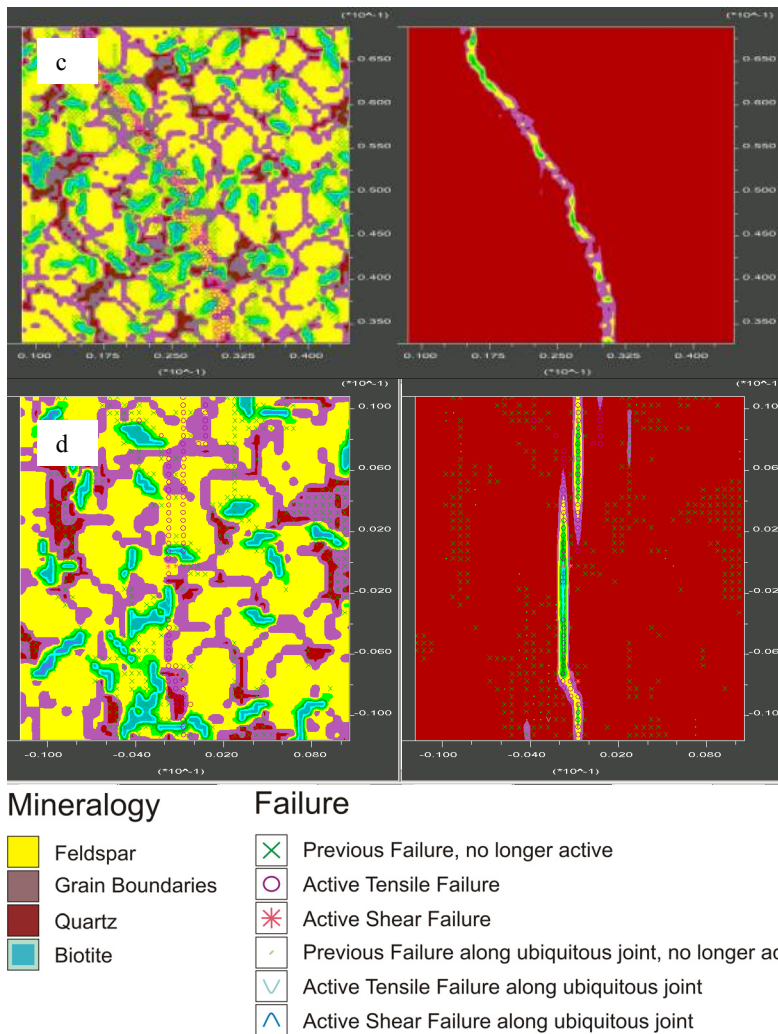
Figure 11 (Continued): c) induced macro fracture through feldspar, quartz and biotite (left) and the shear strain intensity of the corresponding region (right); d) induced tensile fracture through feldspar, quartz and biotite (left) and the shear strain intensity of the corresponding region (right).

4 CONCLUSIONS

4.1 *Discussion of Modelled versus Physical Results*

The UCS and biaxial values are lower in the modelled tests than in the physical tests, in part due to the limitations of simulating a three-dimensional test in 2-D. The hoop stresses that develop in physical UCS models (Diederichs 2003, Diederichs et al. 2004) and likely contribute to higher UCS strength are not developed in the 2-D models. The Brazilian tensile strengths are higher in the modelled tests than in the physical tests, partly due to the continuum nature of the model in which actual breaks in the rock are not developed, in contrast to the physical models in which tensile fractures tear the sample apart with considerable speed and energy, likely contributing to decreased physical strength values. The cohesion values are higher than the physical lab test results with correspondingly lower coefficients of friction, even at low confinement $\sigma_3 < 0.1\sigma_1$, suggesting that the model is not capable of simulating the confinement dependent fracture process. In general, the best fits to UCS, biaxial and Brazilian tensile data require high tensile strength of intact minerals, and low tensile strength and stiffness of fractured minerals. The fits are not perfect, and more work is required to ensure that the models can fit all three tests, particularly the triaxial test at high confining stress.

Improvements to modelled UCS strength could be accomplished by better determining the friction angle and cohesion, and as well as varying the strain rate at which residual friction is mobilised. In particular, increasing the friction angle nearly instantaneously (strain of $1x10^{-8}$) increased the calculated rock friction angle by about 5% with respect to the physical laboratory results from triaxial testing. Further improvements with respect to friction, either in terms of input parameters, mobilisation rate or further explicit mobilisation of macro friction to obtain model biaxial results that are comparable to laboratory triaxial results could be undertaken.

This analysis shows that the constitutive model cannot capture the shearing of minerals that occurs during triaxial failure at high confining stress. A similar phenomenon was observed by Diederichs (1999) in which the peak strength envelope slopes for models of polycrystalline rocks data were much lower than for laboratory test values. The slopes for data points from the crack interaction stress (determined directly in the models) and the axial stress-strain graph non-linearity point were found to have similar slopes in both model and laboratory test data of granite (Diederichs, 1999). It was also found that the peak strength envelopes for laboratory samples loaded very slowly resulted in a much lower slope, approximately 3.8, compared to quickly loaded samples, whose peak strength envelope slope was approximately 7.5.

This suggests that peak values in the biaxial numerical model tests may actually be more representative of the crack initiation threshold, rather than true laboratory peak strength. This phenomenon is particularly important for biaxial model test results since the impact of confining
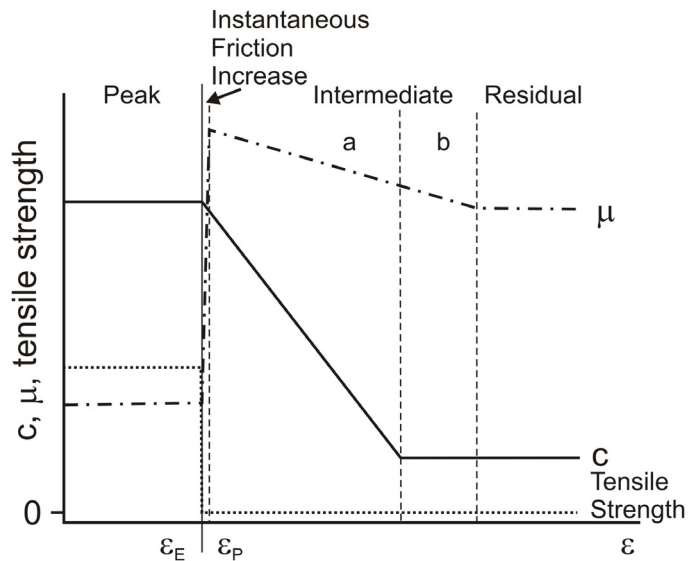
Figure 12: Schematic of strength property (cohesion or friction coefficient, m) and resulting axial strength as it changes with strain, where ε_E and ε_P are accumulated elastic and plastic strain, respectively. Peak strength parameters are used until the element fails and begins to accumulate plastic strain, at which friction increases instantaneously, followed by two levels of intermediate strength parameters (a,b), as a function of increasing plastic strain, until the residual strength parameters are reached.

stress is not correctly modelled, as demonstrated by the lower slope angles of modelled test results. With respect to UCS testing, however, the confining stress is not an issue as the test is undertaken in the unconfined zone of Figure 12, and the behaviour of the model test can be taken as an analogue to the laboratory test. Issues arising from 2-dimensional versus 3-dimensional samples for UCS testing are independent of this phenomenon.

4.2 *Summary of Selected Input Parameters*

Cohesion loss is a small-strain process, while confinement dependent strength arising from friction requires larger strain (Diederichs, 1999). Using this rationale, the cohesion is lost before the mineral has changed to gouge phase (Intermediate a in Fig. 12), and drops to a residual value 1/20 of the peak value. The cohesion loss as a function of strain for input into the FLAC strain

softening constitutive model is determined by estimating the plastic strain at which residual cohesion is reached, using the following relationship for model stability:

$$\varepsilon_{P\_residual} = \frac{cohesion_{peak}}{shear\ módulus} \tag{4}$$

The strain rate used for modelling, is therefore different for each mineral, as well as for maximum and minimum values for the same mineral. Equation 4 defines the relationship between the cohesive strength of the material and the shear stiffness, and expresses the resistance to shearing through an intact mineral lattice in terms of bond strength and bond stiffness. This ratio gives an estimate of the strain required to overcome the shearing resistance. The tensile strength to strain relationship is not so easily determined, but for numerical stability and simplicity, it is associated with the cohesion loss strain rate. The strain level at which mono-mineralic gouge is expected to develop is 10x the strain at which cohesion is lost.

The ranges of values summarised in Table 3 represent the following:
− Cohesion: peak and residual following the values outlined in Section 2.4 and Figure 12.
− Tensile strength: The high-end values result in the best fit for Brazilian and UCS tests calibrated to the Stanstead granodiorite, with instantaneous drop as shown in Figure 12.
− Mineral friction coefficients: base friction coefficient relates to friction of polished mineral surfaces and asperities, as calculated in Section 2.3.
− 'Instantaneous' friction gain to 45º at $\varepsilon = 1x10^{-8}$ in all mineral matrix constitutive models, as shown in Figure 12.
− 'Instantaneous' friction gain to 26º at $\varepsilon = 1x10^{-8}$ in mica ubiquitous joint constitutive models to maintain numerical stability.
− Gouge: monomineralic gouge friction coefficients, as shown in Figure 12.
− Elastic Moduli: low and high are second standard deviation of the normal distribution for quartz and feldspar.

Table 3: Summary of selected FLAC input strength parameters for rock modelling

Mineral	Cohesion (MPa) Peak	Resid.	σ_t (MPa)	Friction Coefficients Base	Gouge	Poisson Ratio	Elastic Moduli (GPa) Young's	Shear	Bulk	Strain $\varepsilon 10^{-3}$ Cohesion Loss
Quartz	109	5	34	0.132	0.65	0.19	47-75	19-31	28-44	3.5 − 5.7
Feldspar	80 – 125	4 – 6	36	0.12 –0 .6	0.8	0.28	72-86	28-33	55-65	4.4 – 2.4
Biotite ‖	48	2	4.5	0.31	0.43	0.18	179	5.8	169	8.3
Biotite ⊥	95	5	39	0.78	0.43	0.053	53	5.8	169	16

5 ACKNOWLEDGEMENTS

6 REFERENCES

Angel, R., Hazen, R., McCormick, T., Prewitt, C., and Smyth, J.E.-. 1988. Comparative compressibility of end-member feldspars. *Physics and Chemistry of Minerals,* 15(4):313-318.

Birch, F. 1966. Compressibility; elastic constants, in Clark, S.P., ed. *Handbook of Physical Constants.* Geological Society of America, New York, pp. 97-174.

Carmichael, R.S. 1982. *Practical Handbook of Physical Properties of Rocks and Minerals.* CRC Press.

Diederichs, M.S. 1999. *Instability of Hard Rock Masses: The Role of Tensile Damage and Relaxation* [Ph.D. thesis]. University of Waterloo, Canada.

Diederichs, M.S. 2003. Rock Fracture and Collapse Under Low Confinement Conditions. *Rock Mechanics and Rock Engineering,* 36(5): 339-381.

Diederichs, M.S., Kaiser, P.K., and Eberhardt, E. 2004. Damage initiation and propagation in hard rock and the influence of tunnelling induced stress rotation. *International Journal of Rock Mechanics and Mining Science*, 41: 785-812.

DeBorst, R. 2002. Fracture in quasi-brittle materials: a review of continuum damage-based approaches. *Engineering Fracture Mechanics*, 69: 95-112.

Fang, Z., and Harrison, J.P. 2002. Application of local degradation model to the analysis of brittle fracture of laboratory scale rock specimens under triaxial conditions. *International Journal of Rock Mechanics and Mineral Science*, 39: 459-476.

Fukuhara, M., Sanpei, A., and Shibuki, K. 1997. Low temperature-elastic moduli, Debye temperature and internal dilational and shear frictions of fused quartz. *Journal of Materials Science*, 32: 1207-1211.

Horn, H.,M., and Deere, D.U. 1962. Frictional Characteristics of Minerals. *Géotechnique*, 12: 319-335.

Itasca Consulting Group Inc. 2007a. *FLAC-Fast Langrangian Analysis of Continua*. Minneapolis, Minnesota.

Itasca Consulting Group Inc. 2007b. *PFC-Particle Flow Code*. Minneapolis, Minnesota.

Lama, R.D., and Vutukuri, V.S. 1978. *Handbook on Mechanical Properties of Rocks*. Trans Tech Publications, Clausthal, Germany, p. 481.

Li, L. 2001. *Microscopic Study and Numerical Simulation of the Failure Process of Granite* [Ph.D. thesis]. University of Lulea.

Li, L., Lee, P.K.K., Tsui, Y., Tham, L.G., and Tang, C.A. 2003. Failure Process in Granite. *International Journal of Geomechanics,* 3(1): 84-98.

Liu, H.Y., Kou, S.Q., and Lindqvist, P. 2002a. Numerical simulation of the fracture process in cutting heterogeneous brittle material. *International Journal for Numerical and Analytical Methods in Geomechanics*, 26: 1253-1278.

Liu, H.Y., Kou, S.Q., Lindqvist, P., and Tang, C.A. 2002b. Numerical modelling of rock fragmentation process induced by multiple indentors. *Proc* NARMS-TAC 2002, Eds. Hammah et al. Toronto, Canada.

Martin, C.D. 1994. *The Strength of Massive Lac du Bonnet Granite Around Underground Openings* [Ph.D. thesis]. University of Manitoba, Canada.

McNeil, L.E., and Grimsditch, M. 1993. Elastic moduli of muscovite mica. *Journal of Physics: Condensed Matter,* 5(11): 1681-1690.

Moore, D.E., and Lockner, D.A. 1995. The role of microcracking in shear-fracture propagation in granite. *Journal of Structural Geology,* 17(1): 95-111.

Morrow, C.A., Moore, D.E., and Lockner, D.A. 2000. The effect of mineral bond strength and adsorbed water on fault gouge frictional strength. *Geophysical Research Letters*, 27 (6): 815-818.

Nasseri, M.H.B., Mohanty, B., and Prasad, U. 2002. Investigation of micro-structural properties of selected rocks and their effect on fracture toughness. *Proc* NARMS-TAC 2002, Eds. Hammah et al. Toronto, Canada. pp. 961-967.

Nasseri, M.H.B., Mohanty, B., and Robin, P.-.F. 2005. Characterization of microstructures and fracture toughness in five granitic rocks. *International Journal of Rock Mechanics & Mining Science,* 42: 450-460.

Patton, F.D. 1966. Multiple modes of shear failure in rock. Proc. 1st congr. Int. Soc. Rock Mech., Lisbon 1, 509-513.

Tang, C.A., and Kaiser, P.K. 1998. Numerical Simulation of Cumulative Damage and Seismic Energy Release During Brittle Rock Failure-Part I: Fundamentals. *International Journal of Rock Mechanics and Mining Sciences*, 35 (2): 113-121.

Tapponier, P., and Brace, W.F. 1976. Development of Stress-Induced Microcracks in Westerly Granite. *International Journal of Rock Mechanics and Mineral Science*, 13: 103-112.

Tromans, D., and Meech, J.A. 2004. Fracture toughness and surface energies of covalent minerals: theoretical estimates. *Minerals Engineering*, 17 (1): 1-15.

Villeneuve, M.C., Diederichs, M.S., and P.K. Kaiser. 2009. Effects of Geomechanical Characteristics on Rock Strength and Spalling Sensitivity. Submitted to *International Journal of Rock Mechanics and Mineral Science*.

Wong, T.-F. 1982. Micromechanics of Faulting in Westerly Granite. International *Journal of Rock Mechanics Mining Science and Geomechanical Abstracts*, 9 (2): 49-64.

Zhu, W.C., and Tang, C.A. 2004. Micromechanical Model for Simulating the Fracture Process of Rock. *Rock Mechanics and Rock Engineering*, 37 (1): 25-56.